Exploring the effects of rooftop mitigation strategies on 1 urban temperatures and energy consumption

Andrea Zonato[1], Alberto Martilli[2], Estatio Gutierrez[3], Fei Chen[4], Cenlin He[4], Michael Barlage[4], Dino Zardi[1], and Lorenzo Giovannini[1]

[1]University of Trento
[2]CIEMAT
[3]University of New York
[4]National Center for Atmospheric Research

November 24, 2022

Abstract

This paper describes and evaluates novel parameterizations for accounting for the effect of rooftop mitigation strategies on the urban environment, in the context of the mesoscale model Weather Research and Forecasting (WRF), coupled with a urban canopy parameterization and a building energy model (BEP+BEM). Through the new implementation, the sensitivity of near-surface air temperature and building energy consumption to different rooftop mitigation strategies is evaluated by means of numerical simulations in idealized urban areas, for typical summer and winter conditions. Rooftop mitigation strategies considered include cool roofs, green roofs and rooftop photovoltaic panels. Results indicate that near-surface air temperature is reduced by all the RMSs during the summer period: cool roofs are the most efficient in decreasing air temperature (up to 1 °C on average), followed by green roofs and photovoltaic panels. Green roofs reveal to be the most efficient strategy in reducing the energy consumption by air conditioning systems, up to 45%, while electricity produced by photovoltaic panels overcomes energy demand by air conditioning systems. During wintertime, green roofs maintain a higher near-surface air temperature than standard roofs. On the other hand, photovoltaic panels and cool roofs reduce near-surface air temperature, resulting in a reduced thermal comfort. The results presented here show that the novel parameterization schemes implemented in the WRF model can be a valuable tool to evaluate the effects of mitigation strategies in the urban environment. The new model is available as part of the public release of WRF in version 4.3.

Exploring the effects of rooftop mitigation strategies on urban temperatures and energy consumption

A. Zonato[1], A. Martilli[2], E. Gutierrez[4], F. Chen[3], C. He[3], M. Barlage[3], D. Zardi[1] and L. Giovannini[1]

[1]Atmospheric Physics Group, Department of Civil, Environmental and Mechanical Engineering,
University of Trento, Trento, Italy
[2]Center for Energy, Environment and Technology (CIEMAT), Madrid, Spain
[3]National Center for Atmospheric Research, Boulder, Colorado
[4]Department of Mechanical Engineering, The City College of New York, New York

Key Points:

- New parameterizations of rooftop mitigations strategies are developed and implemented into the Weather Research and Forecasting (WRF) model
- The new implementations include green roofs and photovoltaic panels, coupled with the BEP+BEM urban canopy models
- Sensitivity tests are conducted in order to evaluate the effect of rooftop mitigation strategies on near-surface air temperature and energy consumption

Corresponding author: Andrea Zonato, `andrea.zonato@unitn.it`

Abstract

This paper describes and evaluates novel parameterizations for accounting for the effect of rooftop mitigation strategies on the urban environment, in the context of the mesoscale model Weather Research and Forecasting (WRF), coupled with a urban canopy parameterization and a building energy model (BEP+BEM). Through the new implementation, the sensitivity of near-surface air temperature and building energy consumption to different rooftop mitigation strategies is evaluated by means of numerical simulations in idealized urban areas, for typical summer and winter conditions. Rooftop mitigation strategies considered include cool roofs, green roofs and rooftop photovoltaic panels. Results indicate that near-surface air temperature is reduced by all the RMSs during the summer period: cool roofs are the most efficient in decreasing air temperature (up to 1°C on average), followed by green roofs and photovoltaic panels. Green roofs reveal to be the most efficient strategy in reducing the energy consumption by air conditioning systems, up to 45%, while electricity produced by photovoltaic panels overcomes energy demand by air conditioning systems. During wintertime, green roofs maintain a higher near-surface air temperature than standard roofs. On the other hand, photovoltaic panels and cool roofs reduce near-surface air temperature, resulting in a reduced thermal comfort. The results presented here show that the novel parameterization schemes implemented in the WRF model can be a valuable tool to evaluate the effects of mitigation strategies in the urban environment. The new model is available as part of the public release of WRF in version 4.3.

Plain Language Summary

The increasing number and duration of heatwaves, is increasing the heat stress for people living in the cities, and largely increase energy resources. To face this problem, the deployment of rooftop mitigation strategies (RMS) such as cool roofs, green roofs, and rooftop photovoltaic panels is starting to be adopted worldwide, with the aim of improving thermal comfort for citizens and diminishing the energy demand for heating/cooling of buildings. This article presents the implementation of new numerical schemes, to consider the effect of the above-mentioned roof mitigation strategies on the urban environment, incorporated with the Weather Research and Forecasting (WRF) mesoscale numerical weather prediction model. Different urban configurations have been investigated, varying the height of the buildings and the distance between them, in order to cover a large spectrum of possible cities. Results show that all rooftop technologies tested in this work increase thermal comfort and diminish energy consumption during summer. The effect of RMS increase with decreasing building height and with increasing building packing density. Results pointed out that advanced parameterization schemes are needed to simulate the feedback between buildings and the atmosphere, which can be used by urban planners to take choices to improve the sustainability of urban areas.

Introduction

It is well known that rooftop technologies, such as cool roofs (CRs), green roofs (GRs) or rooftop photovoltaic panels (RPVPs) can significantly modify fluxes of energy and momentum in the urban canopy layer (Santamouris, 2014). Their deployment is nowadays largely adopted worldwide, with the aim of improving thermal comfort for citizens and diminishing the energy demand for heating/cooling of buildings (Lai et al., 2019). Therefore, a better understanding of the physical mechanisms driving the modifications induced by rooftop mitigation strategies (RMSs) is desirable, for quantifying their effects on the urban environment, for a wide range of urban structures and under different climatic conditions. A better comprehension of these processes is receiving increasing attention from planners and policy makers, especially under growing urbanization and climate change (Chapman et al., 2017). In particular, the increasing number and

duration of heat waves interacts nonlinearly with the well known urban heat island phenomenon (Li & Bou-Zeid, 2013), resulting in extremely high heat stress for citizens and in an increased use of energy resources. On the other hand, cold winters present the same features of heat waves in terms of thermal discomfort and energy demand (Yang et al., 2014), despite cities remain warmer than the surrounding environment. The above-mentioned RMSs have been widely proposed in the literature in the recent years, and their effect have been investigated in different specific case studies. While all RMSs reduce the sensible heat release by roofs (and consequently the heat stored into the building materials), acting on the roof surface energy budget, the mechanisms for GRs, CRs and RPVPs are different. GRs redirect available energy to latent heat at the expense of sensible heat, increasing the evapotranspiration through the vegetation on the rooftop. On the other hand, CRs increase the reflection of the incoming solar radiation by increasing the roof albedo, and preventing the heat storage within roof materials. Finally, PVPs act as screens for the underlying roof, converting part of the incoming solar radiation into electricity. Several studies quantifies the impact of RMSs at the building scale, through field campaigns or numerical simulations (see e.g, Kolokotroni et al. (2013) for CRs, De Munck et al. (2013) for GRs and Dominguez et al. (2011) for PVPs). However, results cannot be simply upscaled to evaluate mitigation effects at the city scale, because the impact of RMSs depends on urban geometry, thermal properties of the building materials and climatic conditions, so a different approach is needed. To this purpose, some recent studies employed mesoscale meteorological models to investigate the city-wide impact of RMSs, adopting urban parameterizations with various levels of complexity. For example, Li et al. (2014) evaluated the city-scale mitigation effect of CRs and GRs over the Baltimore-Washington metropolitan area, using the Weather Research and Forecasting (WRF) model coupled with the Princeton Urban Canopy Model, detecting improvements in terms of air temperature during an heat wave period of the same order of magnitude for the two roof technologies. Yang et al. (2014) incorporated the effect of green roofs in the single layer urban canopy model Noah/SLUCM (Kusaka et al., 2001) and tested it for several megacities, while de Munck et al. (2018) used the Town Energy Balance model (TEB, Masson (2000)), to evaluate the impact of various urban greening scenarios on thermal comfort and energy and water consumption for the city of Paris. For the same city, Masson et al. (2014) demonstrated that PVP arrays can reduce the near-surface air temperature, especially during nighttime. Finally, Salamanca et al. (2016) tested a novel PVP parameterization coupled with the multilayer urban canopy scheme BEP+BEM (Martilli et al. (2002); Salamanca et al. (2010)) for the cities of Phoenix and Tucson, detecting a decrease of both near-surface temperature and energy demand for air conditioning systems (ACSs).

In general, all the above-mentioned studies proposed novel physically-based RMS parameterization schemes, which modify the roof surface energy budget, demonstrating a citywide decrease of air temperature during summer climatic conditions. However, these studies generally lack in generalization, since every RMS parameterization scheme is applied for specific cities under unique climatic conditions. Hence, it is not possible to identify the dependence of the impact of RMSs on urban geometry or atmospheric forcing. Moreover, despite RMSs are worldwide employed to improve thermal conditions in the urban environment during summertime, it is important to evaluate the city-scale effect induced by RMSs also during winter, with the aim of detecting possible reductions in temperatures that may increase thermal discomfort and energy demand for heating systems.

Accordingly, the present study offers a systematic evaluation of the impact of the three above mentioned RMSs (CRs, GRs and RPVPs) on both near-surface air temperature and building energy consumption (EC), for a wide range of idealized urban configurations and for two different climatic conditions. To this purpose, novel schemes have been developed for GRs and RPVPs, and incorporated in the BEP+BEM urban canopy scheme, in the context of the WRF mesoscale meteorological model (v4.1.2, Skamarock et al. (2019)). The modeling system adopted in the present study (WRF coupled with
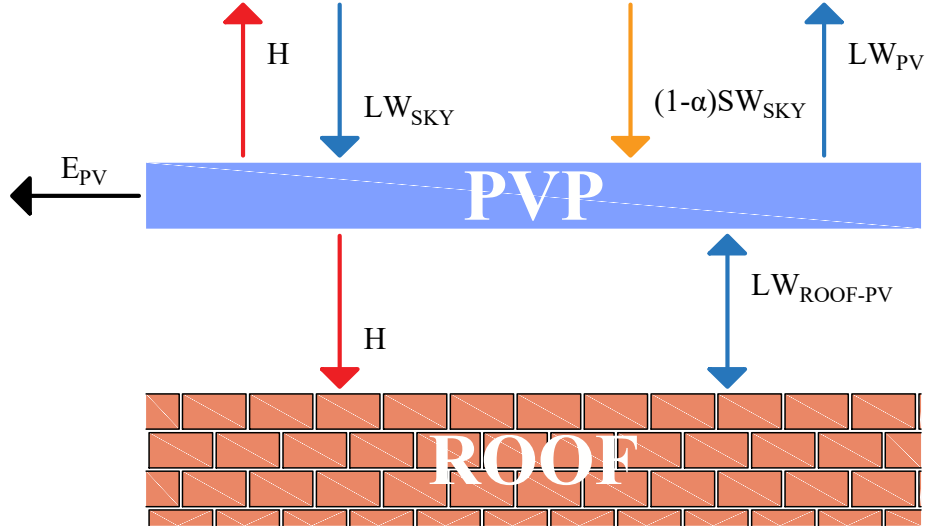
Figure 1: Photovoltaic panel design, with a schematic representation of energy exchanges with the underlying roof and the environment.

BEP+BEM) has been evaluated through the comparison against measurements in several cities, proving to be a suitable tool to reproduce meteorological conditions and EC in urban areas (Giovannini et al. (2014) and Salamanca et al. (2018)).

The paper is organized as follows: Section 1 describes the schemes developed to calculate the surface energy budget of RPVPs and GRs, while Section 2 presents the set-up of the idealized simulations and the methods adopted to conduct the sensitivity analysis. Simulations results are discussed in Section 3, focusing on the comparison between standard roofs and RMSs for different urban configurations and climatic conditions. Finally, results are summarized and discussed in Section 4.

1 The Rooftop Mitigation Strategies schemes

1.1 The Rooftop Photovoltaic Panels parameterization

The parameterization developed in this work in view of taking into account the effects of RPVPs within BEP-BEM share similarities with the models developed by Masson et al. (2014) and Salamanca et al. (2016). Photovoltaic arrays are assumed to be parallel and detached from roofs, and composed of a single layer. Here we calculate the temperature of the PVPs from the energy balance equation (Fig. 1):

$$(1 - \alpha_{PV})SW^{\downarrow}_{sky} + LW^{\downarrow}_{sky} - LW^{\uparrow}_{PV} + LW^{\updownarrow}_{roof-PV} = E_{PV} + H^{\uparrow} + H^{\downarrow} \tag{1}$$

with (all terms in W m^{-2}):

- $(1 - \alpha_{PV})SW^{\downarrow}_{sky}$: net shortwave radiation gained by the upward surface of the PVP, assuming an albedo $\alpha_{PV} = 0.11$.
- $LW^{\downarrow}_{sky}$: incoming longwave radiation at the uppper surface of the PVP;
- $LW^{\uparrow}_{PV} = \varepsilon_{PV}\sigma T^4_{PV} + (1 - \varepsilon_{PV})LW^{\uparrow}_{sky}$: upward longwave radiation emitted and reflected by the PVP, with $\varepsilon_{PV} = 0.93$. T_{PV} is the temperature of the photovoltaic array.

- $LW^{\updownarrow}_{roof-PV} = \frac{1}{\frac{1-\varepsilon_{PV}}{\varepsilon_{PV}} + \frac{1-\varepsilon_{roof}}{\varepsilon_{roof}}} \sigma \left(T^4_{PV} - T^4_{roof} \right)$: longwave ratiation exchanged between the downward face of the PVP and the upward face of the roof. Radiation fluxes coming from the PVP and from the roof are considered together in order to take into account the multiple reflections between the two surfaces.

- $E_{PV} = \eta_{PV} SW^{\downarrow}_{sky} min \left[1, 1 - 0.005 \left(T_{PV} - 298.15 \right) \right]$: energy production by the PVP. It takes into account that the efficiency of PVPs decreases at temperatures higher than 25°C; η_{PV} is the conversion efficiency of the PVP, i.e. the fraction of shortwave radiation converted into electricity. Efficiency varies from 7% for quantum dot cells to 44% for multijunction cells used in research applications (NREL, 2020). In this work, since the most common arrays used for rooftop are mono- and poli-crystalline silicon PVPs, we use an efficiency $\eta_{PV} = 0.15$.

- $H^{\uparrow} + H^{\downarrow} = \left(h^{\uparrow} + h^{\downarrow} \right) \left(T_{PV} - T_{air} \right)$: the sensible heat fluxes at the upward and downward faces of the PVP. The formulation for $h = \sqrt{h_c^2 + a \left| V \right|^b}$ depends on empirical fits and is adopted from the EnergyPlus model (US Department of Energy, 2010), which has been validated against measurements (Scherba et al., 2011). h_c depends on the material of the surface (glass, in this case), on whether the surface faces upward or downward, and on the sign of the difference between surface and air temperature. The absolute value of wind speed is taken at the first level of WRF above the roofs and it is supposed to be the same for the upward and downward face.

While Masson et al. (2014) and Salamanca et al. (2016) parameterized T_{PV} through its dependence on short-wave solar radiation, here we directly solve numerically Eq. (1), in a way similar to Du et al. (2016), through the iterative Newton-Raphson algorithm, to get a PVP temperature that depends on all the involved contributions. When PVPs are present, no solar radiation hits on the roof surface, so short-wave radiation is not considered in the surface energy budget of the roof.

1.2 The Green Roofs parameterization

The land surface scheme for GRs has been developed based on De Munck et al. (2013) and Gutierrez (2015). It calculates energy and water budgets, taking into account incoming net radiation, water input from precipitation and irrigation, evapotranspiration from vegetation, heat exchange with the atmosphere and diffusion of energy and moisture throughout the soil. The model is one dimensional, i.e. horizontal transport and subsurface flows are neglected.

A GR consists of ten layers with a total depth of ~ 0.3 m (Fig. 2). Five levels (0.08 m of total thickness) represent the organic matter substrate where vegetation grows. Vegetation roots reach the bottom of the substrate, and vegetation is assumed to intercept all the incoming radiation from the atmosphere. One layer represents the drainage layer (0.05 m), where surplus water is removed. Finally, four levels describe the insulation layer, composed of a waterproofing membrane (0.003 m), an insulating sheet (0.06 m), a further waterproofing membrane (0.003 m), and finally a layer for insulating the structural roof (0.1 m).

1.2.1 Hydrology for Green Roofs

The latent heat flux LE is modeled considering only evaporation from soil moisture and transpiration through leaves of the water absorbed by roots in the layers composing the substrate:

$$LE = \frac{\rho_a L \left(q_{surf,S} - q_a \right)}{R_a + R_S} \tag{2}$$

where ρ_a is the air density, L the latent heat of vaporization, $(q_{surf,S} - q_a)$ the difference between surface saturated specific humidity and the air specific humidity, R_a the
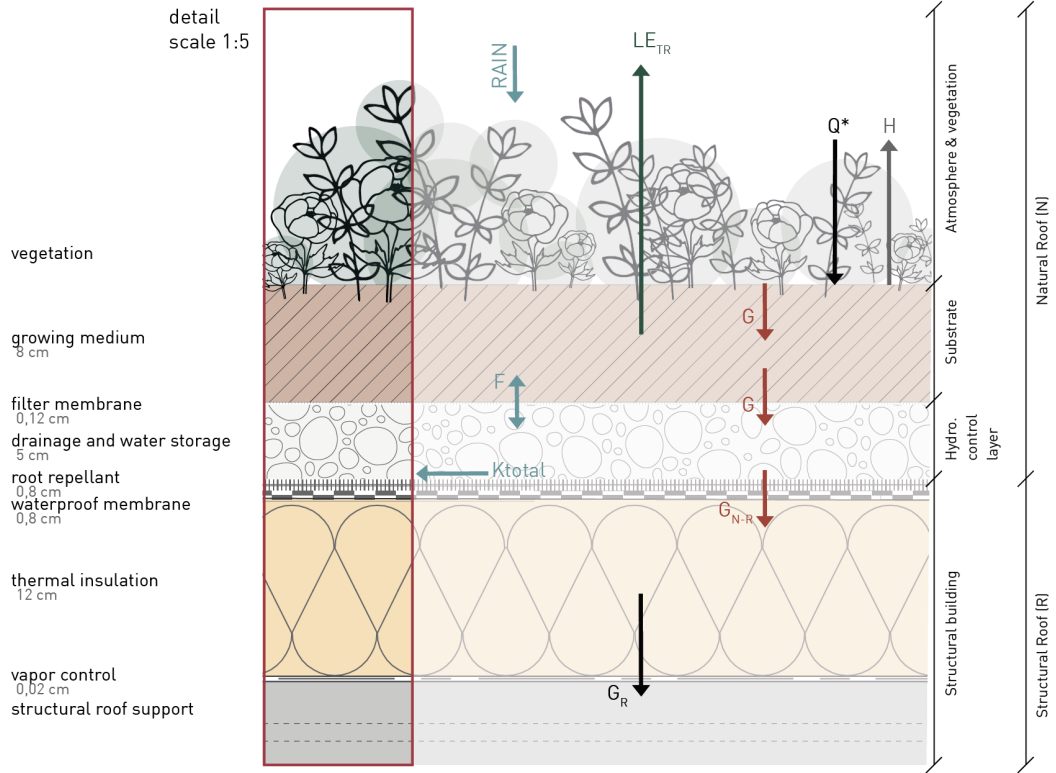
Figure 2: Green roof design. Arrows refers to the sensible/latent heat exchange between the different layers and the atmosphere.

aerodynamic resistance (Louis, 1979) and R_S the stomatal resistance. The latter depends on the atmospheric state, water availability, and vegetation features, and it is written as:

$$R_S = \frac{R_{S_{min}}}{LAI\ F_1 F_2 F_3 F_4} \tag{3}$$

where $R_{S_{min}}$ is the minimum stomatal resistance of the vegetation, while LAI is the leaf area index. F_1 describes the effect of photosynthetic radiation, F_2 the hydrological features, F_3 and F_4 the effect on evapotranspiration of temperature and humidity respectively (see Jacquemin and Noilhan (1990) for more details). The Richards' equation (Short et al., 1995) is used to represent the one-dimensional transport of soil moisture (Θ) throughout the soil:

$$\frac{\partial \Theta}{\partial t} = \frac{\partial}{\partial z}\left(D\frac{\partial \Theta}{\partial z} + K\right) + F_\Theta \tag{4}$$

where D and K are respectively soil water diffusivity and hydraulic conductivity calculated as:

$$K = K_S \left(\frac{\Theta}{\Theta_S}\right)^{2b+3} \tag{5}$$

$$D = \frac{-bK_S\Psi_s}{\Theta}\left(\frac{\Theta}{\Theta_S}\right)^{b+3} \tag{6}$$

187 $\Psi = \Psi_s\left(\frac{\Theta_S}{\Theta}\right)^b$ is the moisture potential, $b = 3.9$ is an empirical coefficient of water
188 retention of organic matter, while all the terms with the subscript "S" refer to the soil
189 in saturation conditions. F_Θ considers all source and sink terms. For the uppermost layer

$F_\Theta = Ir + P - E$, where Ir is the irrigation, P the precipitation rate and E the evapotranspiration. For the drainage layer, just under the substrate, $F_\Theta = -K$ represents the surplus rain drained, if in excess.

1.2.2 Thermodynamics for Green Roofs

The heat transfer between GRs layers is calculated using the Fourier diffusion equation for soil temperature (T):

$$\frac{\partial T}{\partial t} = \frac{\partial}{\partial z}\left(\lambda \frac{\partial T}{\partial z}\right) + F_T \tag{7}$$

where F_T represents source and sink terms. For the uppermost layer F_T is calculated from the surface energy balance:

$$F_T = H - LE + (1 - \alpha_{GR})SW^\downarrow_{sky} + LW^\downarrow_{sky} - LW^\uparrow_{GR} \tag{8}$$

where α_{GR} is the albedo of the GR, and $LW^\uparrow_{GR} = \varepsilon_{GR}\sigma T^4_{GR}$ is the long-wave radiation emission of the GR, with $\varepsilon_{GR} = 0.93$ the emissivity of the GR and T_{GR} its surface temperature. For the layer close to the conventional roof, F_T is the heat conduction flux calculated using the temperature gradient between the bottom layer of the natural roof and the uppermost layer of the structural roof, using a weighted average of their thermal diffusivity. Thermal diffusivity for natural roof layers depends on soil moisture:

$$\lambda = \begin{cases} \frac{e^{-(log_{10}|\Psi|+2.7)}}{C_S} 4.186 \times 10^7 & \text{if } log_{10}|\Psi| \leq 5.1 \\ \frac{4.1 \times 10^{-5}}{C_S} 4.186 \times 10^7 & \text{if } log_{10}|\Psi| > 5.1 \end{cases} \tag{9}$$

where $C_S = (1-\Theta)C_d + \Theta C_w$ is the volumetric specific heat for wet soil, calculated as the weighted average of the volumetric specific heat for dry soil (C_d) and water (C_w).

2 Methodology

2.1 Set-up of the idealized simulations

The set-up of the idealized simulations is similar to the one proposed in Pappaccogli et al. (2020). The effect of different RMSs on air temperature and EC has been evaluated through two-dimensional idealized simulations for various urban geometries and under different meteorological conditions. The idealized simulations, also thanks to their low computational cost, allows investigating a great number of cases, adopting different urban geometries under controlled atmospheric conditions. A total of 168 simulations has been performed for an ideal city situated at a latitude of 45°N. Two different seasons are simulated: a typical summer period (21-23 June, SUM hereafter) and a typical winter period (21-23 December, WIN hereafter), to quantify the effects of rooftop modifications with completely different solar radiation forcing. Simulations consist of a common numerical domain (Fig. 3), composed of 200×3 grid cells with a horizontal spatial resolution of 1 km and 51 vertical grid cells with a finer resolution close to the ground, with 9 cells in the first 110 m. Simulations run with a time step of 10 s, starting at 0000 LST for 72 h. The first 24 h are considered as spin-up period, while the last 48 h are taken into account for the sensitivity analysis. Initial conditions are specified adopting a potential temperature profile with a positive gradient of 3.5 K km^{-1} and a westerly wind with an intensity of 3 m s^{-1} constant with increasing height. Surface temperature is set to 27°C in SUM and to 4°C in WIN averywhere in the domain. Relative humidity is set to 20% and 50% at the surface for SUM and WIN respectively, linearly decreasing to 0% at $\sim$ 5000 m above ground level.

Regarding physics parameterizations, the Bougeault and Lacarrere (1989) scheme is used as Planetary Boundary Layer (PBL) parameterization, while the Noah-MP (Niu et al., 2011) is adopted for land-surface processes. Stamnes et al. (1988) is used for shortwave radiation and the Rapid Radiative Transfer Model (RRTM, (Mlawer et al., 1997))
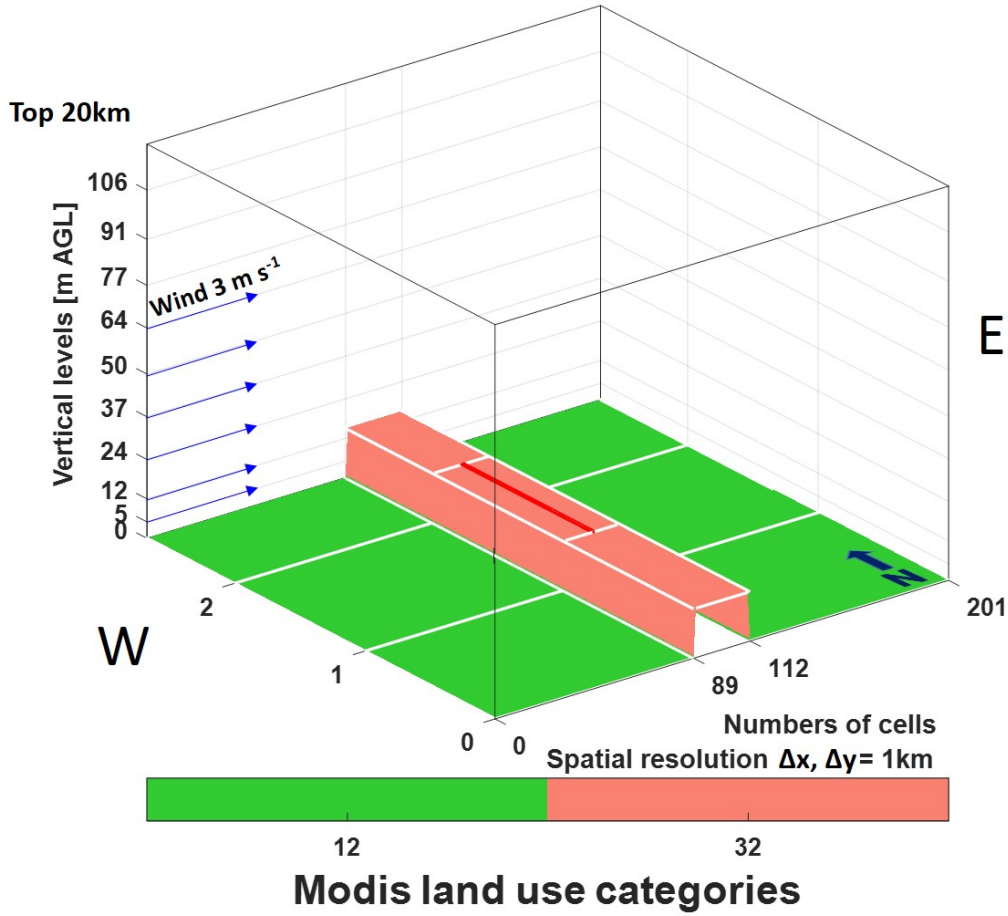
Figure 3: Schematic representation of the domain used for the idealized simulations. The red line represents the cell chosen to analyze the numerical results (from (Pappaccogli et al., 2020))

.

for long-wave radiation. Horizontal turbulent exchange coefficients are kept constant and equal to 300 m^2 s^{-1}. Finally, microphysics and cumulus schemes are turned off, to avoid the formation of clouds. Periodic lateral boundary conditions are set for all the input variables, in both N-S and W-E directions.

A 23-km wide city is situated in the center of a completely flat domain, while the surrounding rural areas are classified as "cropland", according to the MODIFIED_ IGBP_MODIS_NOAH classification in WRF. The width of the city is the same for all the simulations, as well as buildings and urban ground thermal properties. Since this work aims at quantifying the impact of different mitigation strategies on air temperature and EC, several geometrical building features are tested, to consider a large spectrum of possible urban configurations. In Fig. 4, the schematic representation of all the scenarios simulated in this work is shown. For all the simulations, the building width B is set to 10 m, and artificial surfaces are supposed to occupy the entire cell, hence the urban fraction is set to 1. Urban geometry in the simulations varies depending on building height, which is set to 5, 10, and 20 m, and building surface to total surface fraction, defined as $\lambda_p = B/(B+S)$,
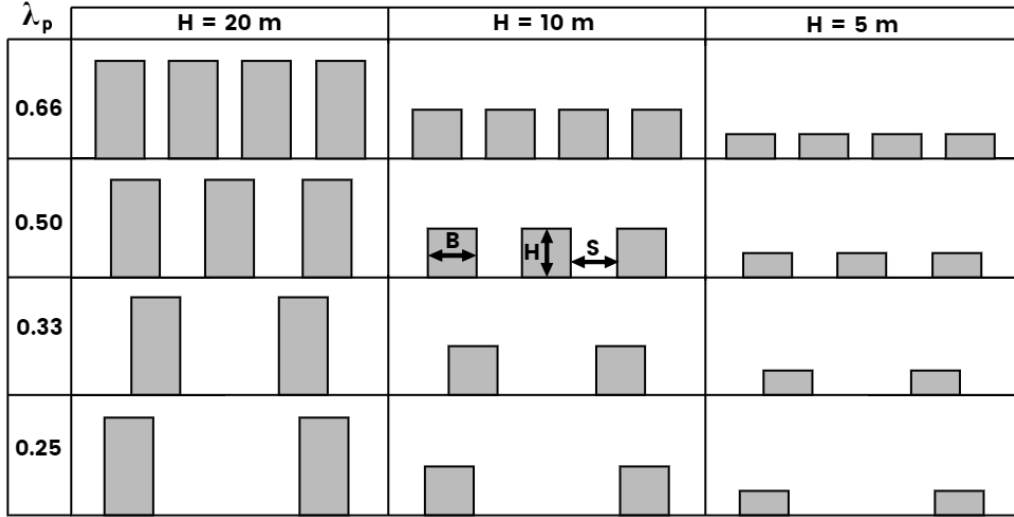
Figure 4: Schematic representation of the 12 different urban configurations for the idealized simulations. B is the building width, S the street width, H the building height and λ_p the building area to total area ratio.

where S is the street width. λ_p varies with the street width, that is set, ranging from scattered to packed configurations, equal to 30, 20, 10 and 5 m, resulting in $\lambda_p = 0.25$, 0.33, 0.50 and 0.66 respectively. This range in λ_p has been identified by (Grimmond & Oke, 1999) as representative of most of the cities worldwide. Hence, the 12 possible building geometric configurations represent a wide range of Local Climate Zones, from residential areas with low and scattered buildings, to city centers with high and compact buildings. For all the simulations, thermal and physical properties of buildings are kept constant (Tab. 1). In particular, building walls are assumed to be composed of solid brick, with windows covering 20% of the surface, while roofs are covered with clay tiles. For ground, we adopt thermal parameters of asphalt (values are taken from Oke et al. (2017)). SUM and WIN differs in indoor target temperature. It is set to 20°C for WIN and to 25°C for SUM, according to the directive UNI/TS 11300–1 (UNI/TS 11300–1, 2014; Pappaccogli et al., 2018). Internal temperature fluctuations of ± 2°C are permitted, and it is prescribed that the heating/cooling system is on during the whole time of the simulations. For WIN a coefficient of performance (COP) of 0.9 is adopted, which represents the average energy efficiency of most heating systems (i.e. gas and fuel fired boilers, electrical resistance heaters, heat pumps etc., (Martilli, 2014)), while for SUM it is set to 3.5, representing the typical coefficient of performance of the ACS. In order to estimate the energy consumed per person (and to calculate the heat generated by inhabitants), 0.02 person m^{-2} are assumed within buildings, a typical value for European cities (Eurostat, 2018).

2.2 Sensitivity analysis

In this work, we quantify the effect of several RMSs with respect to standard roofs (STD), taken as reference simulation for each urban configuration, for a total of 12 different urban geometries (combination of three building heights and four λ_p). In particular, a total of six RMSs are tested, as here summarized:

- Cool Roof (CR): for this scenario, the standard roof albedo (Tab. 1) is replaced with $\alpha = 0.80$;

Table 1: Thermal and physical parameters for the idealized simulations.

	Roof	Walls	Road
Heat Capacity (MJ m^{-3} K^{-1})	1.77	1.37	1.94
Thermal Conductivity (W m^{-1} K^{-1})	0.84	0.83	0.75
Albedo	0.30	0.35	0.15
Emissivity	0.90	0.90	0.95
Target Temp. for ACs (°C)	25 (SUM), 20 (WIN)		
Percentage of windows	20%		
Persons per area (person m^{-2})	0.02		

- Green Roof with grass (GRASS): the standard roof is supposed to be completely covered with a green roof, as shown in Fig. 2. The GR is covered by grass, assuming $LAI = 2$, $\alpha_{gr} = 0.154$, $R_{S_{min}} = 40$ and initial green roof soil moisture $SM = 0.2$ m^3 m^{-3};
- Green Roof with sedum (SEDUM): same as GRASS, but in this case the GR is covered with sedum, assuming $LAI = 3$, $\alpha_{gr} = 0.3$, and $R_{S_{min}} = 150$. Sedum is more frequently used for GRs in dry climates, due to their ability to withstand long periods of heat and water stress by partially closing their stomata during the day (De Munck et al., 2013);
- Green Roof with grass and irrigation (GRASS+IRRI): same as GRASS, but assuming to irrigate the GR vegetation in the period 0100-0300 LST. A total of 25 L m^{-2} of water per week (as in de Munck et al. (2018)) is set at the surface of the uppermost GR layer;
- Photovoltaic panels (PVP): photovoltaic panels with albedo $\alpha = 0.11$ and efficiency $\eta_{PV} = 0.15$ (Salamanca et al., 2016) are assumed to be superimposed over all the roofs, detached from them.
- Green Roof with grass and photovoltaic panels (GRASS+PVP): same as GRASS, but with the GR covered with PVPs. Radiation is assumed not to reach the vegetation, hence the GR is completely in the shadow of the PVPs.

3 Results

In this section the differences in 2-m air temperature and EC between the simulations implementing the RMSs and STD are evaluated. Results are analyzed considering both the full diurnal cycles, to understand when RMSs are more effective, and the average differences over all the simulation period, to evaluate which is the best mitigation strategy and with which urban configuration. Finally, the analysis focuses on temperature and energy budget time series at the roof level, to understand the physics governing each RMS. Results are presented separately for SUM and WIN, to better understand the effects of the RMSs in the two seasons. Since the diurnal cycles of the variables considered here are very similar on the two days analyzed, we decided to average both days into a single diurnal cycle, to cancel out random fluctuations and obtain more robust results.

3.1 Summertime

Figure 5 shows the diurnal cycle of 2-m air temperature (left) and EC by air conditioning per person (right) for the central cell representing the idealized city in the STD simulations. The solid line represents the mean value of the different simulations, while
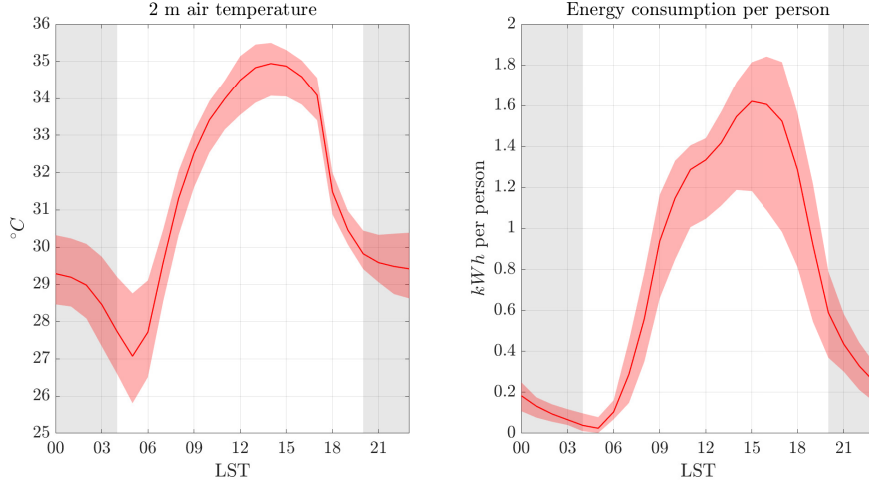
Figure 5: Summertime average air temperature at 2 m AGL (left) and energy consumption per person (right) averaged over a single diurnal cycle for the STD simulations (red line). The red shaded regions represent the variability obtained in the simulations with different urban configurations. Shaded background indicates nighttime hours

the variability is shown by the shaded regions. On average, a maximum temperature of ~ 35°C is reached at 1400 LST, while minimum temperature is ~ 27 °C at 0500 LST. These temperature values are representative of typical climatic conditions during a strong heatwave in an urban area at mid latitudes. Temperature variability between different urban configurations is low during daytime, while it becomes larger during nighttime, because of the strong influence of the urban geometry on UHI intensity during nighttime (Martilli (2014),Zonato et al. (2020)). EC is very low during nighttime, when indoor temperature decreases below the target value and ACSs are not needed, while it reaches its maximum around 1500 LST (~ 1.6 kWh per person), shifted by one hour with respect to the 2-m air temperature peak, due to the thermal inertia of building materials. The variability of EC between different urban configurations is higher during daytime with respect to temperature variability, since EC for each cell does not depend only on external temperature, but has a strong dependence also on urban morphology, and in particular on the number of floors in each cell. In fact, buildings with more than one floor exhibit a lower EC per person, since overlaying floors insulate lower floors and reduce heat dispersion in the vertical direction.

3.1.1 Impact on 2-m air temperature

Figure 6 shows the time series of 2-m air temperature differences between the STD scenario and all the RMSs for all the possible urban configurations. A feature common to all RMSs is a decrease in temperature for all configurations, with higher differences for lower buildings (the roof surface is closer to the ground, so the effect of the RMSs is more intense) and higher λ_p (the cooling effect increases as a larger ground surface is covered by buildings). For all RMSs, the diurnal cycles in Fig. 6 are mainly driven by radiation: the largest mitigation effect takes place in the central hours of the day (1100-1300 LST), when less available radiation is converted into sensible heat, and slightly decreases reaching the sunset. During the first hours of the night, when sensible heat stored in building materials starts to be released, RMSs affect air temperature, due to the reduced storage of heat within buildings. However, their effect rapidly vanishes around sunrise (0500-0600 LST), when small positive differences (i.e. higher temperatures) are present,
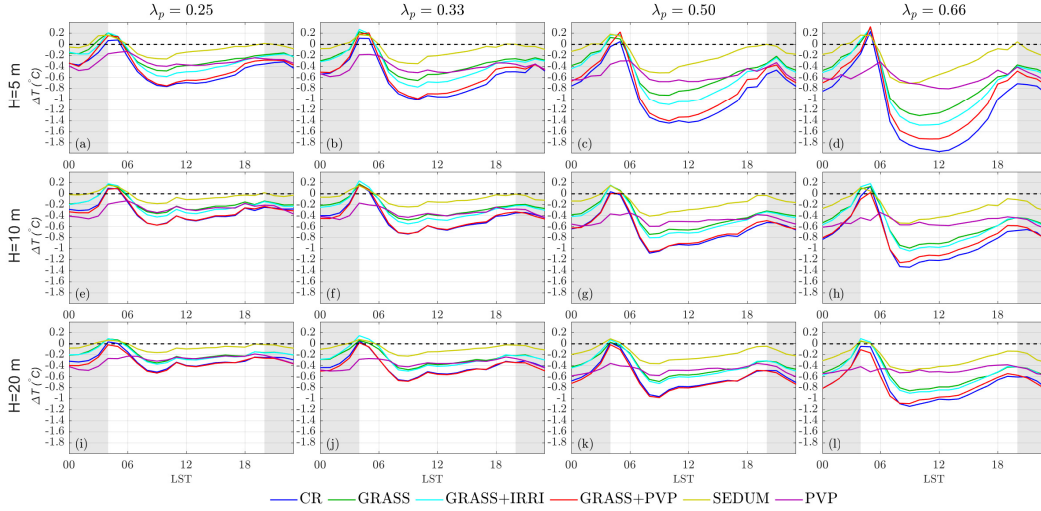
Figure 6: Summertime 2-m air temperature differences between STD and each RMS, averaged for the central urban cell, and for a single diurnal cycle. Building height is kept constant along the rows, while λ_p along the columns. Shaded background indicates nighttime hours.

except for the PVP case. This is due to the larger temperature gradients between roof surfaces and air, and, as a consequence, higher sensible heat fluxes, as will be shown in Section 3.1.3.

Quantifying the effect of RMSs, the higher impact is detected in the H = 5 m, λ_p = 0.66 configuration (panel (d)), with a maximum reduction of $\sim$ 1.9°C at 1200 LST for CR and of $\sim$ 1.8°C at 1100 LST for GRASS+PVP. They are followed by GRASS+IRRI and GRASS, which reduce the temperature during the peak of solar radiation of $\sim$ 1.4°C and $\sim$ 1.2°C respectively. The difference between these two cases, i.e. with and without irrigation, increases as the simulation time advances: indeed, while for GRASS the soil moisture contininues to diminish, for GRASS+IRRI the soil moisture is periodically increased by irrigation (not shown). SEDUM and PVP display an average temperature reduction of $\sim$ 0.8°C, with the peak at 1300 LST for the latter. Despite SEDUM and GRASS share the same roof design, the different type of vegetation deployed on the roof changes the impact on the surface energy balance. Grass is more efficient with respect to sedum in converting solar radiation to latent heat flux, resulting in a lower outgoing sensible heat flux. While from 0600 to 1900 LST GRs and CRs are the most effective RMSs, from 0300 to 0600 LST PVP becomes the most efficient, since this simulation does not show a marked reduction of temperature difference around sunrise as in the others RMSs.

In order to quantify the average effect of the different RMSs varying the urban configuration, 2-m air temperature differences are averaged for all the period of simulation and compared for each building height (Fig. 7). As said before, CR is the most effective RMS, with an average reduction of $\sim$ 1.2°C, followed by GRASS+PVP, with a reduction of $\sim$ 1°C for the configuration with H = 5 m and λ_p = 0.66 (panel (c)). In general, all the RMSs show a quasi-linear decrease of temperature with increasing λ_p, with increasing negative slope as the efficiency of the RMS increases. For example, for 5-m high buildings the difference between CR and SEDUM is of $\sim$ 0.3°C for λ_p = 0.25 and of $\sim$ 0.9°C for λ_p = 0.66. With increasing building height the effect of the RMSs diminishes, and so does also the difference between the slopes. PVP is the only RMS that does not show a linear trend with λ_p: while for $\lambda_p < 0.5$ the temperature reduction is higher
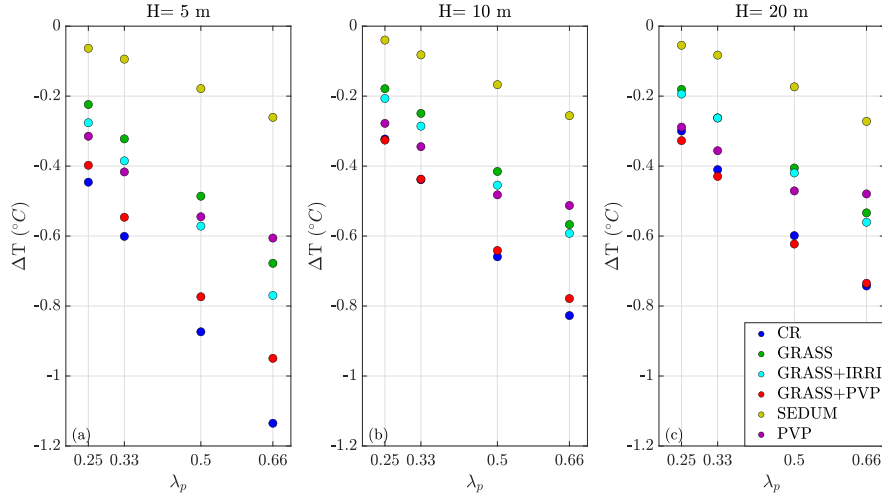
Figure 7: Summertime 2-m air temperature differences for each RMS averaged over all the period of simulations, depending on λ_p. The left panel shows 5-m building configurations, central panel 10-m buildings, and right panel 20-m buildings.

than in GRASS and GRASS+IRRI, for $\lambda_p = 0.66$ its effect is lower than in GRASS and GRASS+IRRI, indicating a saturation of the mitigation effect at high λ_p values.

While linearity of mitigation is evident with respect to λ_p, temperature reduction is not linear with decreasing building height: if λ_p is kept constant, the difference in temperature reduction between H = 5 m and H = 10 m is higher compared to that observed between H = 10 m and H = 20. Again, SEDUM is the least efficient strategy in mitigating 2-m air temperature, since this type of vegetation converts less radiation into latent heat flux with respect to all the simulations with grass. Focusing on GRASS and GRASS+IRRI, it is possible to notice that GRASS+IRRI is slightly more efficient in reducing 2-m air temperature: assuming to irrigate the GR during nighttime, the latent heat flux during daytime will be higher with respect to the case without irrigation, resulting in a reduced sensible heat flux release. Moreover, if we assume to deploy a photovoltaic layer over the green roof, the combined effect of the PVP and of the vegetation makes this RMS comparable with CR.

3.1.2 Impact on energy consumption

Figure 8 shows the time series of the differences in EC per person between STD and all the RMSs for all the possible urban configurations. Also in this case it can be seen that the effect of the RMSs increases with increasing λ_p and with decreasing building height. RMSs impact is more significant in the floor close to the roof, therefore a higher reduction of EC is found for low buildings, composed of a single floor, than for higher buildings, where the effect on lower floors is lower. The different RMSs do not affect EC in the same way they affect air temperature: the largest reduction occurs at 1500 LST for CR, coincident with the EC peak, and at 1700 LST for simulations with GRs and for PVP. The shift in time of the maximum difference is probably linked to the higher thermal inertia of insulating waterproof layers of which the GRs are made, and to the screening effect of the PVPs. All the simulations implementing GRs show a similar maximum reduction in EC, by ~ 0.8 kWh per person for H = 5 m, larger than the decreases in CR (~ 0.6 KWh per person) and PVP (~ 0.3 kWh per person). However CR displays a higher EC reduction in the night and in the morning. It is remarkable that, despite different types of vegetation and soil moisture, GR cases show the same reduction in EC.
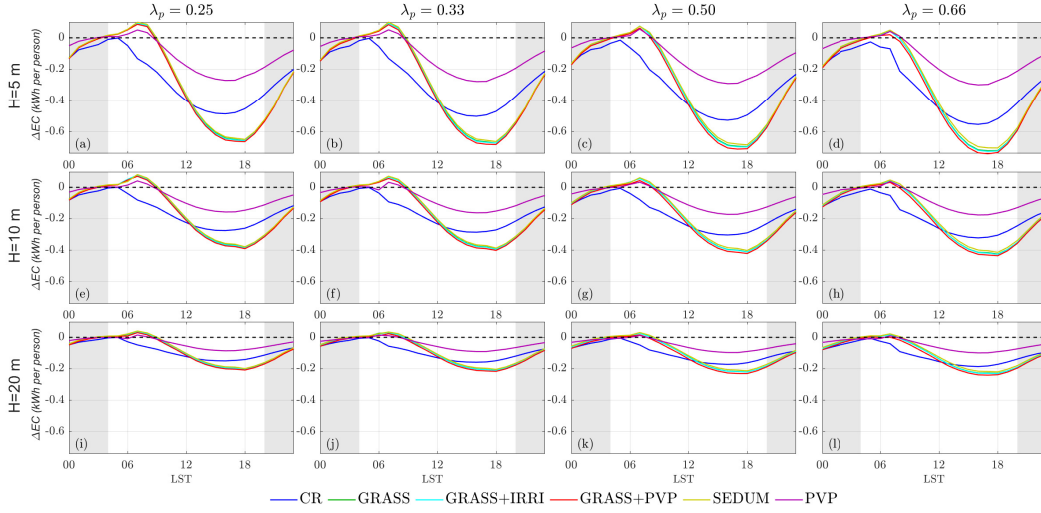
Figure 8: Differences in energy consumption per person between STD and each RMS averaged for the central urban cell and for a single diurnal cycle during summertime. Building height is kept constant along the rows, while λ_p along the columns. Shaded background indicates nighttime hours.

Table 2: Summertime energy saving per person on average and in percentage by PVP simulations including electricity produced by photovoltaic modules.

H \ λ_p	0.3	0.5	1	2
5 m (kWh per person)	-2.25 (-312%)	-2.25 (-316%)	-2.26 (-329%)	-2.27 (-354%)
10 m (kWh per person)	-1.13 (-152%)	-1.14 (-157%)	-1.14 (-173%)	-1.14 (-194%)
20 m (kWh per person)	-0.57 (-80%)	-0.57 (-86%)	-0.58 (-99%)	-0.58 (-117%)

This means that the impact of the insulating waterproof layer, which prevents heat from penetrating into the roof, is more important than the effect of the different surface energy balance. If the energy produced by PVPs is neglected in the net computation of EC, the PVP case is the least efficient in diminishing EC, since PVPs act as a screen for shortwave radiation, but they also transmit heat to the underlying roof through infrared radiation.

In Fig. 9, the cumulative difference in EC per person is shown for each RMS, expressed as percentage with respect to the STD case, for all the period of simulation and for each urban configuration. The EC decreases linearly with growing λ_p for all the RMSs: this linearity is mainly due to the linear decrease of 2-m air temperature, that contributes to diminish the EC by ACSs. As shown in Fig. 8, all the simulations implementing GRs perform similarly in reducing EC, with a cumulative decrease comparable to the CR case. While CR and simulations with GRs can diminish EC up to 30-45% for 5-m buildings, PVP is less efficient in reducing EC, with values up to 13-18%. In fact, while CRs prevent 80% of radiation to reach the roof, PVPs reflect only 11% of radiation and convert an additional 15% into electricity. Therefore, radiation entering the surface energy budget is almost four times higher in PVP with respect to CR. Moreover, no additional insulating layers as in the simulations with GRs are implemented in PVP, resulting in a
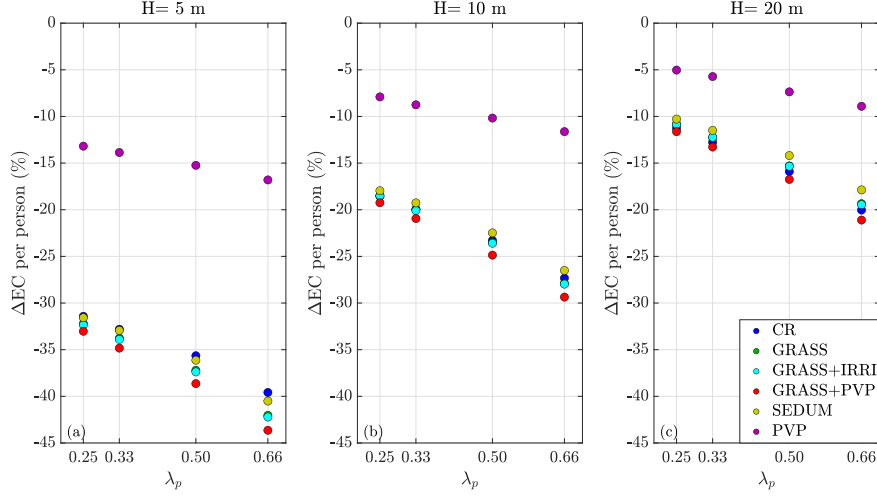
Figure 9: Variation (percentage) in energy consumption per person with respect to the STD case, for each RMS for all the period of simulation during summertime, depending on λ_p. The left panel shows results for 5-m buildings, the central panel for 10- m buildings and right panel for 20-m buildings.

higher heat flux through the roof layers. However, if we assume to instantly use electricity produced by PVPs for the ACSs energy supply, we have a surplus of energy with respect to consumption (if the energy saving in Table 2 is less than -100%, the production overcomes the demand). In the worst case scenario (H = 20 m, λ_p = 0.25), the production of electricity allows a decrease of EC of $\sim 80\%$ (-0.57 kWh per person on average), while for H = 5 m and λ_p = 0.66, each building consumes around one third of the total energy produced by PVPs (2.25 kWh per person on average), under the assumption that the roof surface is totally covered by PVPs.

3.1.3 Temperatures and energy budget at the roof level

Figures 10 and 11 show the diurnal cycles of air and roof temperatures and of surface fluxes, respectively, for a roof situated in the center of the city, for all the simulations in the configuration with H = 10 m and λ_p = 0.50. This configuration has been chosen as an example to highlight the effects of the RMSs on the surface energy budget and on air and roof temperatures. Considering STD, surface temperature reaches its maximum value ($\sim 45°$C) around noon, with a corresponding maximum in the outgoing sensible heat flux of ~ 400 W m^{-2}. On the other hand, the peak of the internal roof layer temperature is reached at 1700 LST ($\sim 36°$C), due to the thermal inertia of building materials. During nighttime surface roof temperature is always lower than the temperature of the internal layer, reaching a minimum value of $\sim 25°$C at 0400 LST.

CRs have a significant impact on surface temperature, with maximum values reaching $\sim 34°$C, i.e. 12°C less than the standard roof, influencing also near-surface air temperature. Also the temperature of the internal roof layer is diminished by 4°C, causing the decrease of EC. In this case, the sensible heat flux is almost null during nighttime and in the first hours of the day, and it becomes positive only in the late morning. Regarding the scenarios implementing GRs, it is clear that the emission of latent heat flux from vegetation and natural soil is the principal factor in diminishing air temperature. Looking at GRASS, the maximum temperature of vegetation is lower with respect to the standard roof temperature by $\sim 5°$C, especially in the first part of the day. Moreover, the latent heat flux always overcomes the sensible heat flux. The peak of latent heat flux
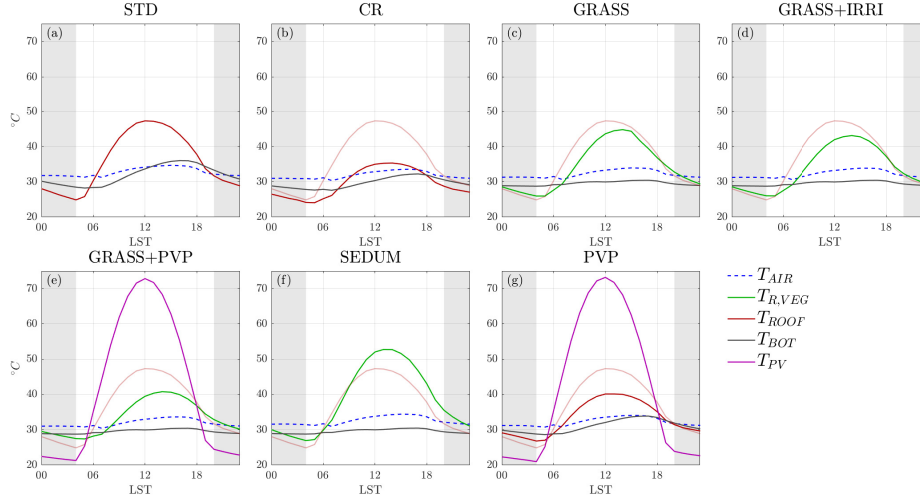
Figure 10: Summertime temperature diurnal cycles of first air layer above the roof (dashed blue), vegetated roof surface (green), upper roof layer (red), lower roof layer (gray), and PVP (purple), for the central cell representing the city, for the configuration with H = 10 and λ_p = 0.50. The temperature of the upper roof layer of STD is represented in pink also in the other panels for comparison. Shaded background indicates nighttime hours.

occurs at noon, one hour before the peak of sensible heat flux: this means that the impact of vegetation is more marked in the earlier hours of the day, resulting in a higher difference with respect to standard roofs during this period, when also 2-m air temperature differences are larger, as shown in Fig. 6. Also the temperature of the internal roof layer is lower (~ 5°C) with respect to STD: in this case, the waterproof insulating layers of the green roof prevent the heat to diffuse through building materials, and hence inside building rooms. This is evident also observing the indoor sensible heat flux, which is almost null for all the cases with GRs. Differences in magnitude between sensible and latent heat flux are even bigger in the GRASS+IRRI case, since irrigation contributes to increase the soil moisture of the GR, and hence to increase the latent heat flux. On the other hand, since sedum is less efficient in converting solar radiation into latent heat flux with respect to grass, the roof temperature in SEDUM is similar to the one of STD, but with higher values in the second part of the day, probably because of the reduced diffusion of heat towards the internal layers of the roof, due to the waterproof insulating layers. However, the temperature of the internal roof layer in SEDUM is comparable to the one in GRASS, strengthening the hypothesis that processes taking place within the building are not significantly affected by the vegetation type, but rather by the thermal properties of building materials.

Focusing on the PVP case, the panel temperature reaches very high maximum values (~ 70°C), corresponding to the peak of solar radiation. Despite a considerably higher temperature with respect to the environment, the outgoing heat flux from the PVP is lower with respect to the one from the standard roof surface, because the material constituting the PVP is less efficient in releasing heat. As a consequence, the sum of the sensible heat flux from the PVP and the roof is lower than the sensible heat flux in STD. This means that, despite the higher temperature of the PVP with respect to the standard roof, the reduced total sensible heat flux diminishes air temperature with respect to STD. Moreover, the shading effect exerted by the PVP on the roof, despite the long-wave radiation exchange between the two surfaces, decreases the surface temperature of
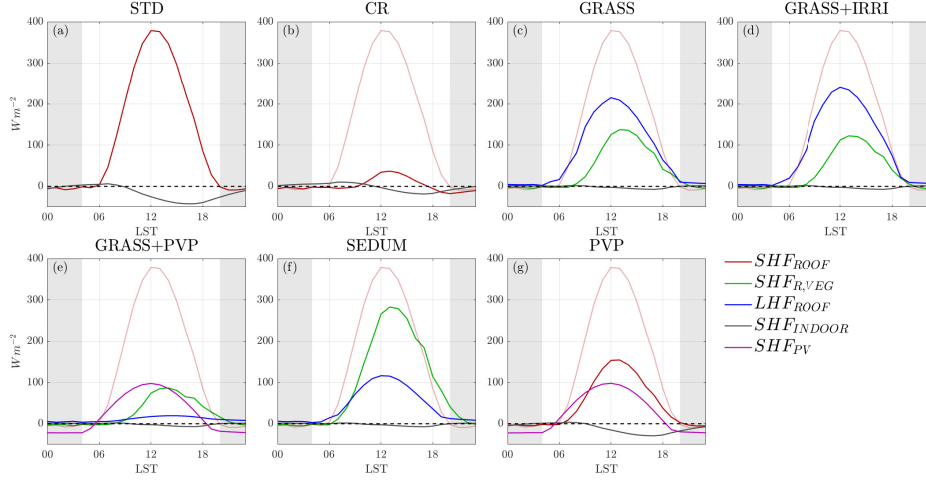
Figure 11: Summertime diurnal cycles of sensible heat flux for standard roof (red), vegetated roof (green), indoor (grey), PVP (purple) and of latent heat flux for vegetation (blue), for the central cell representing the city, for the configuration with H = 10 and λ_p = 0.50. The sensible heat flux of STD is represented in pink also in the other panels for comparison. Shaded background indicates nighttime hours

the roof by $\sim 5°C$, resulting in a lower EC by buildings during daytime. On the other hand, during nighttime, PVP temperature is lower than both air and roof temperature, resulting in a negative heat flux (i.e. heat goes from the environment to the PVP), contributing in decreasing air temperature during nighttime. Similar results, from experimental campaigns, are shown by Broadbent2019 (over bare soil) and Dominguez2011 (over a flat roof). In both studies, the temperature of the PVP is $\sim 30°C$ higher during daytime and $\sim 10°C$ lower during nighttime with respect to the one of the underlying surface.

No substantial differences with respect to PVP are shown by GRASS+PVP, considering both heat fluxes and the temperature of the PVP; this means that the heat exchange processes are not significantly influenced by the characteristics of the underlying surface. On the other hand, shading affects the heat exchange between vegetation and the atmosphere: vegetation temperature in GRASS+PVP is slightly lower during daytime than in GRASS, because there is no radiation reaching the vegetation.

3.2 Wintertime

Figure 12 shows the diurnal cycle of 2-m air temperature (left) and EC per person due to space heating (right) during wintertime for the central cell representing the idealized city in the STD simulations. On average, the maximum temperature reached by the simulations is $\sim 6°C$ at 1300 LST, while the minimum value is $\sim 1°C$ at 0800 LST depicting, as expected, a lower diurnal variability than the summer scenario. Temperature variability between different urban configurations is again larger during nighttime, due to the dependence of the UHI effect on urban geometry, with a range of $\sim 4°C$ between the different urban configurations. EC trend with time is opposite with respect to the summer case: EC is minimum, with even null values for some urban configurations during the central hours of the day, when solar radiation warms building materials, while it increases during nighttime, keeping a quasi-constant value from 0000 to 0600 LST. Also in this case EC variability between different urban configurations is higher with respect to temperature variability.
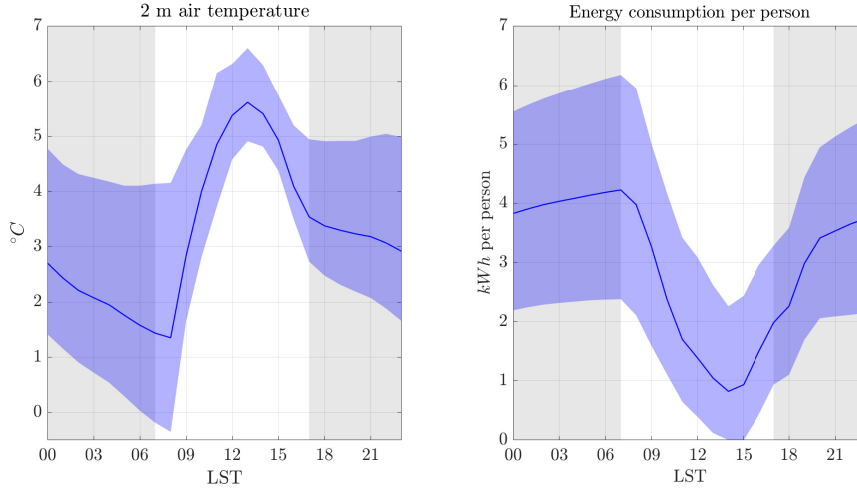
Figure 12: Wintertime average air temperature at 2 m AGL (left) and energy consumption per person (right) averaged over a single diurnal cycle for the STD simulations (blue line). The blue shaded regions represent the variability obtained in the simulations with different urban configurations. Shaded background indicates nighttime hours

3.2.1 Impact on 2-m air temperature

Figure 13 shows the time series of 2-m air temperature differences between STD and all the RMSs for all the possible urban configurations. It is worth noting that, opposite to the summer season, during wintertime a higher temperature is beneficial both for thermal comfort and for EC. Figure 13 shows that in winter not all the RMSs decrease 2-m air temperature, as was highlighted for the summer season (Fig. 5). In general, temperature in the simulations implementing GRs is higher than in STD, especially during nighttime, while CR and PVP display a decrease in air temperature. The peak of temperature decrease for CR coincides with the peak of solar radiation, while for PVP the effect is larger during nighttime. For all the RMSs and all the urban configurations, the differences with respect to STD are smaller than in the summer case: being winter solar radiation considerably lower than during summertime, also the modification of the surface energy budget induced by the RMSs is less significant in winter than in summer. Also in this case the highest differences with respect to STD occur in urban configurations with higher λ_p and lower buildings. In general, simulations with PVPs exhibit the lowest temperatures, especially during nighttime, with a decrease in 2-m air temperature up to ~ 0.8°C. This is probably due to the shadowing effect of the PVP, that avoids the storage of heat within the roof, with a consequent minor release during nighttime, and to the low temperature of the PVPs, inducing a negative heat flux (see Section 3.2.3). The diurnal cycle of 2-m air temperature differences for CR is similar to the summer case, with the highest negative difference at noon ($\sim$ -0.6°C for most cases). On the other hand, during nighttime CR maintains a temperature ~ 0.1°C lower than STD, and differences become null at sunrise. Therefore, the negative effect caused by the temperature decrease is less significant in CR with respect to PVP, since it acts especially during daytime. Simulations implementing GRs present the highest dissimilarities compared to the summer case: while during the central hours of the day (when thermal comfort is higher than at nighttime) 2-m air temperature differences with STD are negative ($\sim$ -0.4°C for all the configurations with $\lambda_p = 0.66$), in the evening and during nighttime all simulations with GRs show a higher temperature than STD, up to ~ 0.4°C for SEDUM. The increase in temperature, which is beneficial for both thermal comfort and EC, is mainly due to the
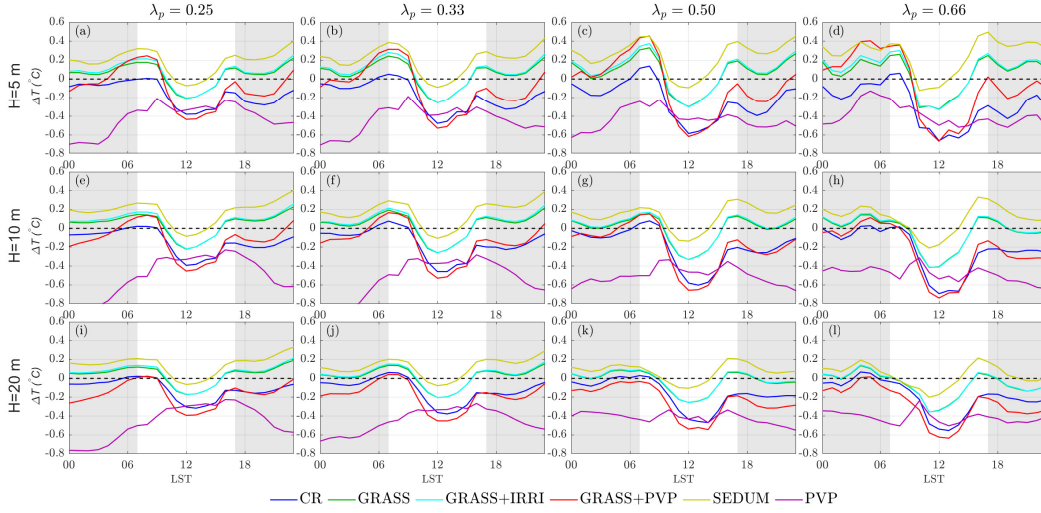
Figure 13: Wintertime 2-m air temperature differences between STD and each RMS, averaged for the central urban cell, and for a single diurnal cycle. Building height is kept constant along the rows, while λ_p along the columns. Shaded background indicates night-time hours.

combination of the higher thermal capacity of the GR with respect to the standard roof (heat stored during daytime, and released in higher amounts during nighttime) and to the low latent heat flux during daytime (the low winter radiation never makes the latent heat flux to overcome the sensible one, as shown in Fig. 18). This is due to the fact that the stomatal resistance is inversely proportional to the solar radiation and consequently the conversion of solar radiation into latent heat is less favoured during wintertime. The effect of the reduced latent heat is clear if we refer to SEDUM: sedum vegetation is less efficient in converting solar radiation into latent heat flux, therefore this RMS is the one that shows the highest temperature differences with respect to STD. Finally, GRASS+PVP behaves similarly to the other simulations with GRs during nighttime, while during daytime the shadowing of the PVPs causes a reduction of the 2-m air temperature.

On average (Fig. 14), 2-m temperature differences induced by the RMSs slightly increase with increasing λ_p for the H = 5 m cases (with the exception of PVP), while they are almost constant for H = 10 m. On the contrary, simulations exhibit a decrease of 2-m temperature differences with increasing λ_p for H = 20 m (with the exception of CR). SEDUM is the RMS which shows the largest increase in temperature, and thus the largest benefit in terms of thermal comfort, up to $\sim$ 0.2°C for the configuration with λ_p = 0.66 and H = 5 m. GRASS+PVP is influenced by the reduction in temperature induced by the PVP, with positive differences ($\sim$ 0.1°C) for H = 5 m and a reduction of $\sim$ 0.1°C for H = 10 m and H = 20 m. Finally, differences in CR and PVP are always negative. PVP shows the highest decrease in temperature (and thus the worst impact on thermal comfort), with values of $\sim$ -0.5°C for all the simulations. It can also be observed that positive differences (cases with GRs) decrease with increasing building height, while negative differences (CR and PVP) assume similar values for all the heights considered, hence the negative effect due to the temperature decrease does not depend on the building height.
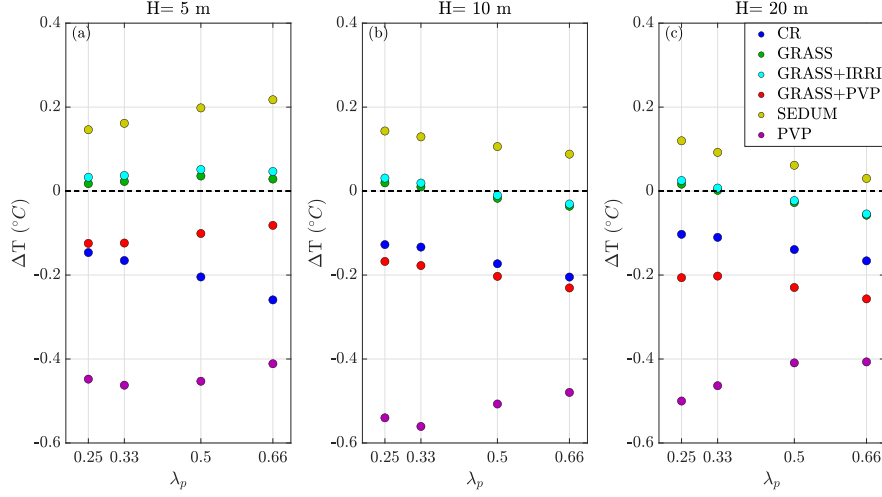
Figure 14: Wintertime 2 m air temperature differences for each RMS averaged over all the period of simulations, depending on λ_p. The left panel shows 5-m building configurations, the central panel 10-m buildings, and the right panel 20-m buildings.

3.2.2 Impact on energy consumption

Figure 15 shows the time series of the differences in EC per person due to space heating between STD and all the RMSs for all the urban configurations. Since EC is low during daytime, the effect of the RMSs takes place mainly during nighttime hours. During the night, at constant H (i.e. for each row of Fig. 15) the differences in EC induced by the variation of λ_p are very low, due to fact that temperature differences are not influenced by this parameter (cf. Fig. 14). The influence of GRs on EC does not depend on the type of vegetation and on soil moisture, since all the simulations with GRs show the same trend. In particular, while during daytime the differences with STD are small, from 0000 to 0600 LST all simulations with GRs depict a constant decrease in EC, up to 2.5 kWh per person for the H = 5 m cases, where the effect is stronger, since buildings are composed of a single floor. Concerning CR, there is always an increase in EC by heating, especially for low buildings. Differences are almost null or slightly positive during nighttime, when the modified roof albedo does not affect the energy budget of the roof surface, while they display a maximum around 1600 LST, due to the reduction of the roof surface temperature. The results for PVP are similar during daytime, with a small increase in EC by heating, but lower in magnitude than in CR. On the other hand, from 0000 to 1000 LST in PVP there is a decrease in EC: while during daytime PVPs reduce roof surface temperature, during nighttime they trap the infrared radiation emitted by the roof, keeping it warmer than in STD (see Fig. 17)

Figure 16 shows the cumulative differences in percentage of EC by heating per person between all RMSs and STD for all the simulations. As shown above,for the same building height, differences are almost insensitive to λ_p. Therefore, contrary to the summer case, street width does not influence the effect of RMSs on EC. Regarding PVP, differences are always negative but close to zero ($\sim 5\%$ for the H = 5 m cases); this is due to the compensation of increased EC during daytime and reduced EC during nighttime. In Table 3 the energy saving per person, in percentage and on average over the period of integration, in the PVP simulations is shown, assuming to instantly use the energy produced by the photovoltaic modules for heating: in contrast to the summer case, during wintertime electricity production never overcomes energy demand, due to the fact that
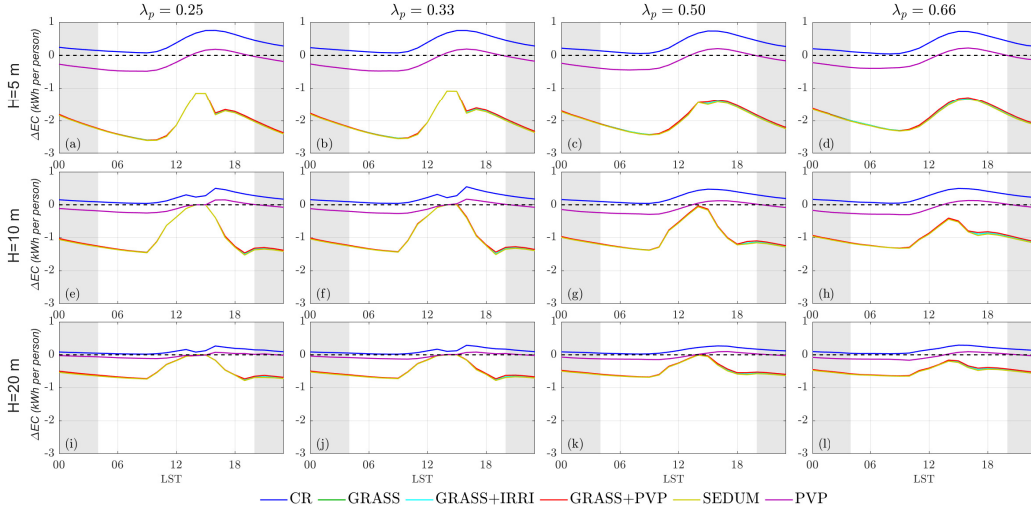
Figure 15: Differences in energy consumption per person between STD and each RMS averaged for the central urban cell and for a single diurnal cycle during wintertime. Building height is kept constant along the rows, while λ_p along the columns. Shaded background indicates nighttime hours (Notice that the range of the axes is different varying the building height).

Table 3: Wintertime energy saving per person on average and in percentage by PVP simulations including electricity produced by photovoltaic modules.

λ_p / H	0.3	0.5	1	2
5 m (kWh per person)	−0.73 (−17%)	−0.72 (−17%)	−0.69 (−17%)	−0.68 (−15%)
10 m (kWh per person)	−0.36 (−14%)	−0.36 (−14%)	−0.37 (−14%)	−0.38 (−15%)
20 m (kWh per person)	−0.16 (−9%)	−0.17 (−9%)	−0.18 (−11%)	−0.19 (−12%)

the energy produced by PVPs is lower than during summertime, due to the lower incoming solar radiation. The maximum reduction is of 0.73 kWh per person, compared to 2.25 kWh per person in the summer period, roughly three times higher). In particular, the maximum percentage saving of $\sim 17\%$ is reached for the H = 5 m cases, while for 20-m tall buildings, EC can be reduced by up to 12%. On the other hand, CR always increases EC by $\sim 10\%$ for all the urban configurations. Again, all simulations with GRs show a relevant saving of EC by heating. In particular, the combined effect of insulation by waterproof layers and higher thermal capacity consents a saving in EC up to $\sim 40\%$ for the H = 5 m cases, and a reduction of EC of $\sim 30\%$ and $\sim 25\%$ for the H = 10 m and H = 20 m cases respectively. As in the summer case, there are no relevant differences induced by the GR vegetation type or the soil moisture availability, indicating that the insulating layers are the dominating effect in reducing EC by heating.

3.2.3 Temperatures and energy budget at the roof level

Figures 17 and 18 show the time series of air and roof temperature and of heat fluxes respectively, for the configuration with $\lambda_p = 0.50$ and H = 10 m for the winter season,
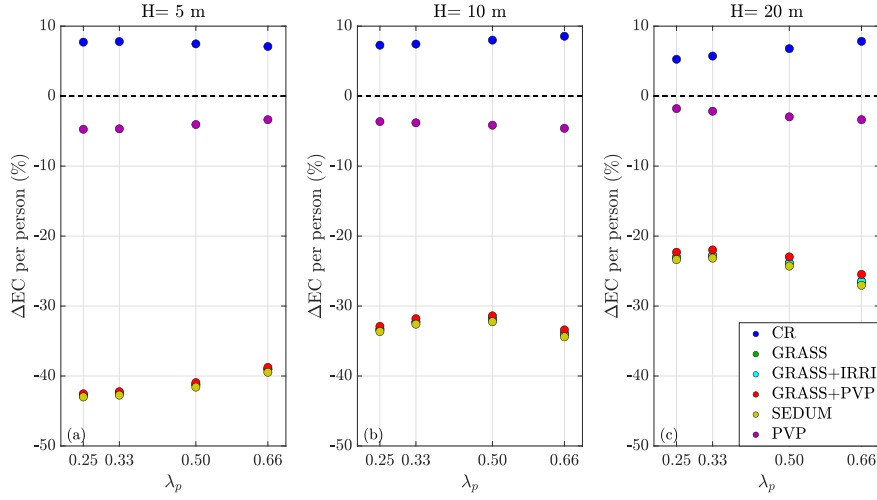
Figure 16: Variation (percentage) in energy consumption per person with respect to the STD case, for each RMS for all the period of simulation during wintertime, depending on λ_p. The left panel shows results for 5-m buildings, the central panel for 10- m buildings and right panel for 20-m buildings.

for all the simulations. Considering STD, as in the summer season, roof temperature is higher than air temperature during daytime and lower during nighttime, reaching a maximum temperature of $\sim 10°C$ at 1300 LST and a minimum value of $\sim 0°C$ after sunset. Contrarily to the summer case, the temperature of the internal roof layer is always higher than both air and roof surface temperature, since a target temperature of 20°C is required for the building rooms. The temperature of the internal roof layer oscillates between $\sim$ 10°C during nighttime and $\sim 14°C$ during daytime, always lower than the target temperature. Since the temperature of the internal roof layer is always higher than the external surface temperature, indoor sensible heat flux is always outgoing (i.e. from the internal room to the environment), with minimum values during daytime, when radiation heats the roof. CR behaves as in the summer case: roof temperature is reduced, and it is always comparable with air temperature. Internal roof temperature is lower than STD, especially during daytime. During daytime PVP acts similarly to CR: the PVP prevents the radiation to reach the roof surface, thus the roof is cooler than in STD, despite the PVP temperature reaches $\sim$ 17°C. On the other hand, during nighttime, the roof, shielded by the PVP, is warmer ($\sim 5°C$) than STD. PVP temperature during nighttime is much lower than air temperature, with differences of $\sim 5°C$, with a resulting negative PVP sensible heat flux ($\sim$ -20 W m^{-2}) and lower air temperature with respect to STD. Simulations with GRs instead show an increase of roof surface temperature with respect to STD, especially after 1300 LST and during nighttime. In this time period GRs are warmer than STD by $\sim 5°C$ due to the combination of i) the reduced upward latent heat flux (almost null even during daytime), due to a lower incoming short-wave radiation in the winter season with respect to summertime and ii) the higher thermal capacity of the GR layers with respect to the standard roof, resulting in a reduction of the upward sensible heat flux during daytime, and an increase during nighttime. In fact, while the peak of the upward sensible heat flux in STD is $\sim$ 100 W m^{-2}, the peak in the simulations with GRs is $\sim$ 60 W m^{-2} and shifted in time, due to the higher thermal inertia. Moreover, just after sunset, the upward sensible heat flux assumes slightly positive values, increasing outdoor temperature, as seen in Sec. 3.2.1. The effect of insulating waterproof layers is again clear looking at the temperature of the internal roof layer, that is constantly warmer than in STD by $\sim 7°C$, and from the indoor sensible heat flux, that
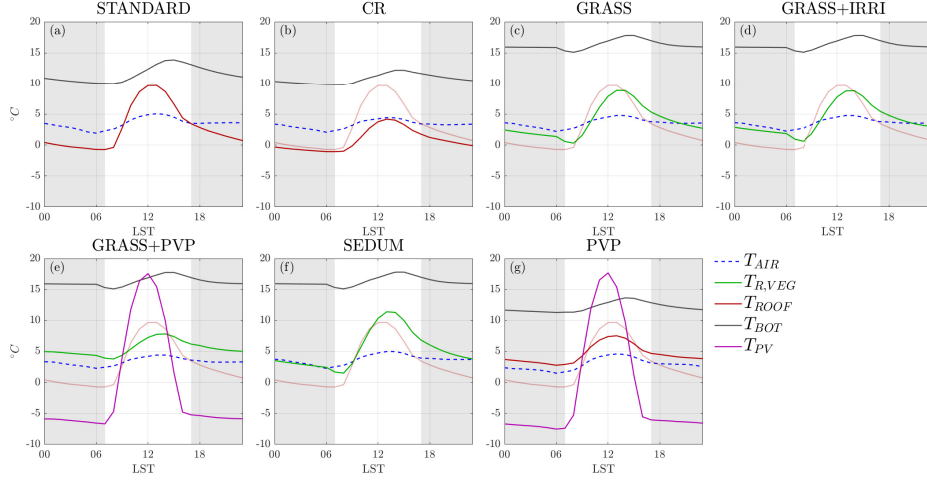
Figure 17: Wintertime diurnal cycle of temperature of near-surface air (dashed blue), vegetated roof (green), upper roof layer (red), lower roof layer (gray) and PVP (purple), for the central cell representing the city, for the $H = 10, \lambda_p = 0.50$ configuration. The temperature of the upper roof layer of STD is represented in pink also in the other panels for comparison. Shaded background indicates nighttime hours.

oscillates around zero. Regarding SEDUM, the lower efficiency in converting radiation into latent heat flux with respect to grass is beneficial during wintertime, since roof surface temperature is higher than in GRASS, and contributes to increase air temperature. Finally, GRASS+PVP highlights the negative effects of PVP during daytime (decrease of roof temperature with respect to STD), and the benefits of GRs during nighttime (higher roof temperature and thermal insulation that prevents the dissipation of heat through the roof layers).

4 Discussion and conclusions

This study presented the results of two-dimensional idealized simulations with the mesoscale WRF model in the urban environment, implementing innovative parameterizations of RMSs, coupled with the BEP-BEM urban parameterization schemes. In particular, simulations were performed under two different climatic conditions (i.e. summertime and wintertime), for twelve different urban configurations, with the aim of quantifying the effect of different RMSs, i.e. cool roofs, green roofs and rooftop photovoltaic panels, on 2-m air temperature and on EC, for several urban geometries. Below we summarize the key results, highlighting the main differences between simulations implementing rooftop mitigation strategies and a simulation with standard roofs, taken as the reference:

- *Dependence of air temperature on urban configuration.*
  The mitigation effect on air temperature varies almost linearly with the building surface to total surface fraction (λ_p) during summertime, while in wintertime it linearly increases only for 5-m high buildings. The mitigation effect is higher for low buildings, with a non-linear decrease of the impact with building height. Therefore, the urban configuration with the lowest buildings and the highest λ_p (H = 5 m and $\lambda_p = 0.66$) shows the highest effect of the RMSs.
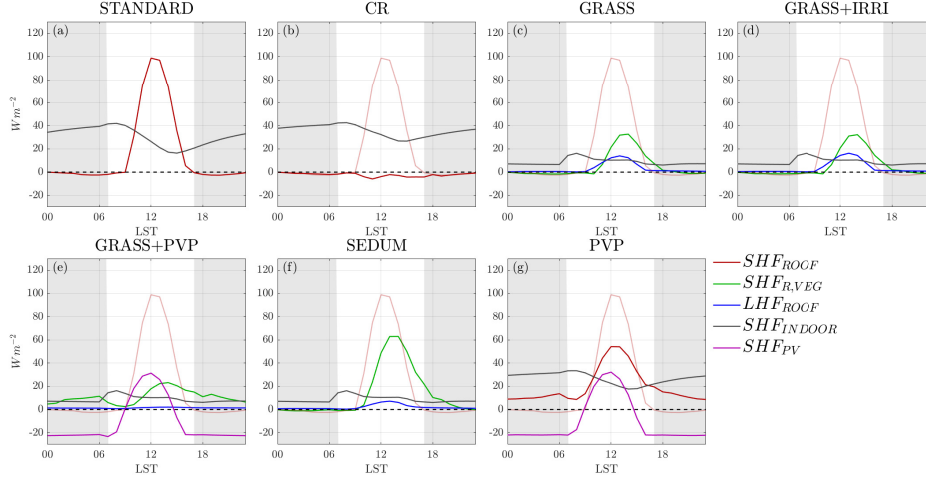- *Dependence of energy consumption on urban configuration.*

Figure 18: Wintertime diurnal cycle of sensible heat flux for standard roof (red), vegetated roof (green), indoor (grey), PVP (purple) and of latent heat flux for vegetation (blue), for the central cell representing the city, for the $H = 10, \lambda_p = 0.50$ configuration. The sensible heat flux of STD is represented in pink also in the other panels for comparison. Shaded background indicates nighttime hours.

During summertime, similarly to temperature, the saving of EC per person by ACSs induced by RMSs increases linearly with λ_p, and decreases with building height, since RMSs act mostly on the floor just below the roof. During wintertime, instead, no dependence of EC by heating with varying λ_p was detected. As in the summer case, the energy saving percentage decreases as the building height increases.

- *Temperature mitigation during summertime*
  All mitigation strategies induce a decrease in air temperature with respect to the standard roof, with a greater effect during daytime. For all the RMSs, the highest temperature reduction occurs at 1000 LST and lasts for all the day, with the exception of the period close to sunrise, apart for PVP. In general, CR is the most efficient in reducing summer temperatures, with a maximum decrease of $\sim 1.8°$C and a daily average decrease of $\sim 1°$C for the urban configuration with $H = 5$m and $\lambda_p = 0.66$. The second most efficient RMS is GRASS+PVP, thanks to the superposition of the beneficial effects of PVPs and of the GR. GRASS and GRASS+IRRI performs similarly, with a slightly lower temperature for GRASS+IRRI, because of the larger latent heat flux release due to the higher soil moisture (average mitigation of $\sim 0.7°$C). SEDUM is the RMS with the smallest impact on air temperature: sedum vegetation is less efficient in converting solar radiation into latent heat flux, hence the mitigation effect is in general less than half with respect to GRASS. PVP temperature decrease, during daytime, is comparable to SEDUM for most urban configurations. However, during nighttime, since PVP reduces the heat stored within the building materials, it maintains a lower temperature even at sunrise (differently from the other RMSs), resulting, on average, as efficient as GRASS.

- *Energy consumption during summertime*
  In general, all RMSs decrease EC by ACSs, with the maximum saving during the late afternoon. All simulations implementing GRs show the same behaviour, since for EC the dominant feature is the insulating effect of the waterproof layers constituting the GR (and not the vegetation type), and they are the most efficient

during daytime. The effect of CR is lower with respect to the simulations with GRs during daytime, while during nighttime hours it overcomes all the other RMSs, because the increased albedo avoid the storage on heat within the roof. On average, CR and simulations with GRs are comparable in terms of energy saved (-45% for the urban configuration with H = 5 m and $\lambda_p = 0.66$), while PVP ensures a saving up to 15%. If we assume to employ all the electricity produced by PVPs for the ACSs supply, we obtain a net gain for all urban configurations, with a energy production up to $\sim 350\%$ of the EC for 5-m buildings.

- *Temperature mitigation during wintertime*
  Contrary to summertime, during wintertime RMSs are beneficial if they induce an increase of air temperature. During wintertime, CR and PVP act similarly to the summer period, i.e. diminishing temperature during all the day, with higher reductions during daytime, corresponding to the peak of solar radiation. However, since during wintertime solar radiation forcing is weaker, the reduction is limited to up to ~ 0.3 °C for CR, around six time less than in summertime, and ~ 0.4 °C for PVP. On the other hand, all simulations with GRs perform differently with respect to summertime. Since the latent heat flux is greatly reduced, because of the dependence of stomatal resistance on solar radiation, more energy is stored into building materials. As a consequence, more heat is released during nighttime: since sedum vegetation is the less efficient in triggering evapotranspiration, SE-DUM is the most efficient in warming up during wintertime, with an average increase of ~ 0.2°C for the configuration with H = 5 m and $\lambda_p = 0.66$.

- *Energy consumption during wintertime*
  The temperature decrease induced by CR during wintertime causes an increase in EC by heating of $\sim 10\%$ for all the urban configurations. On the other hand, PVP slightly decreases the energy demand, because of the screen effect induced by the PVP for infrared radiation during nighttime, despite lower outdoor temperatures. The electricity produced by PVPs is not sufficient to cover all the EC by heating, due to the lower energy production from the low incoming solar radiation. All the simulations with GRs, because of the combined effect of increased external temperatures and of the insulating layer (that prevents the diffusion of indoor heat through the roof), reduce EC up to 40% for the urban configurations with H = 5 m (assuming an initial indoor temperature equal to the target temperature).

The aim of this study was to quantify the effect of various rooftop mitigation technologies under different climatic conditions, in order to set a benchmark for urban climate studies. A wide range of urban configurations under two typical climate scenarios was investigated, so as to provide a comprehensive set of results, that can be representative of most mid-latitude cities. Results pointed out that advanced parameterization schemes are needed to simulated the complex feedback between buildings and the atmosphere, in order to obtain reliable results, that can be used by urban planners and decision-makers to take informed choices to improve the sustainability of urban areas.

Data Availability Statement

Simulations output can be found at: Zonato, Andrea (2021): SIMULATIONS SUMMER. figshare. Dataset. `https://figshare.com/articles/dataset/SIMULATIONS_SU MER/14282420` and Zonato, Andrea (2021): SIMULATION WINTER. figshare. Dataset. `https://figshare.com/articles/dataset/SIMULATIONS_WINTER/14282177` while the code will be included into the WRF version 4.3.

References

Bougeault, P., & Lacarrere, P. (1989, aug). Parameterization of Orography-

Induced Turbulence in a Mesobeta–Scale Model. *Monthly Weather Review*, *117*(8), 1872–1890. Retrieved from `http://journals.ametsoc.org/doi/abs/10.1175/1520-0493(1989)117{\%}3C1872:POOITI{\%}3E2.0.CO;2http://journals.ametsoc.org/doi/abs/10.1175/1520-0493{\%}281989{\%}29117{\%}3C1872{\%}3APOOITI{\%}3E2.0.CO{\%}3B2` doi: 10.1175/1520-0493(1989)117⟨1872:POOITI⟩2.0.CO;2

Chapman, S., Watson, J. E. M., Salazar, A., Thatcher, M., & McAlpine, C. A. (2017, oct). The impact of urbanization and climate change on urban temperatures: a systematic review. *Landscape Ecology*, *32*(10), 1921–1935. Retrieved from `http://link.springer.com/10.1007/s10980-017-0561-4` doi: 10.1007/s10980-017-0561-4

De Munck, C., Pigeon, G., Masson, V., Meunier, F., Bousquet, P., Tréméac, B., . . . Marchadier, C. (2013). How much can air conditioning increase air temperatures for a city like Paris, France? *International Journal of Climatology*, *33*(1), 210–227. doi: 10.1002/joc.3415

de Munck, C., Lemonsu, A., Masson, V., Le Bras, J., & Bonhomme, M. (2018). Evaluating the impacts of greening scenarios on thermal comfort and energy and water consumptions for adapting Paris city to climate change. *Urban Climate*. doi: 10.1016/j.uclim.2017.01.003

Dominguez, A., Kleissl, J., & Luvall, J. C. (2011). Effects of solar photovoltaic panels on roof heat transfer. *Solar Energy*, *85*(9), 2244–2255. doi: 10.1016/j.solener.2011.06.010

Du, Y., Fell, C. J., Duck, B., Chen, D., Liffman, K., Zhang, Y., . . . Zhu, Y. (2016). Evaluation of photovoltaic panel temperature in realistic scenarios. *Energy Conversion and Management*, *108*, 60–67. Retrieved from `http://dx.doi.org/10.1016/j.enconman.2015.10.065` doi: 10.1016/j.enconman.2015.10.065

Eurostat. (2018). *Living conditions in Europe, 2018 edition.* doi: 10.2785/39876

Giovannini, L., Zardi, D., de Franceschi, M., & Chen, F. (2014, mar). Numerical simulations of boundary-layer processes and urban-induced alterations in an Alpine valley. *International Journal of Climatology*, *34*(4), 1111–1131. Retrieved from `http://doi.wiley.com/10.1002/joc.3750` doi: 10.1002/joc.3750

Grimmond, C. S. B., & Oke, T. R. (1999, sep). Aerodynamic Properties of Urban Areas Derived from Analysis of Surface Form. *Journal of Applied Meteorology*, *38*(9), 1262–1292. Retrieved from `http://journals.ametsoc.org/doi/abs/10.1175/1520-0450{\%}281999{\%}29038{\%}3C1262{\%}3AAPOUAD{\%}3E2.0.CO{\%}3B2` doi: 10.1175/1520-0450(1999)038⟨1262:APOUAD⟩2.0.CO;2

Gutierrez, E. (2015). *Quantification of environmental impacts of heat fluxes from built environments* (Unpublished doctoral dissertation). The City University of New York.

Jacquemin, B., & Noilhan, J. (1990). Sensitivity study and validation of a land surface parameterization using the HAPEX-MOBILHY data set. *Boundary-Layer Meteorology*, *52*(1-2), 93–134. doi: 10.1007/BF00123180

Kolokotroni, M., Gowreesunker, B., & Giridharan, R. (2013, dec). Cool roof technology in London: An experimental and modelling study. *Energy and Buildings*, *67*, 658–667. Retrieved from `http://dx.doi.org/10.1016/j.enbuild.2011.07.011https://linkinghub.elsevier.com/retrieve/pii/S0378778811003136` doi: 10.1016/j.enbuild.2011.07.011

Kusaka, H., Kondo, H., Kikegawa, Y., & Kimura, F. (2001). A Simple Single-Layer Urban Canopy Model For Atmospheric Models: Comparison With Multi-Layer And Slab Models. *Boundary-Layer Meteorology*, *101*(3), 329–358. Retrieved from `https://doi.org/10.1023/A:1019207923078` doi: 10.1023/A:1019207923078

Lai, D., Liu, W., Gan, T., Liu, K., & Chen, Q. (2019, apr). A review of mitigat-

ing strategies to improve the thermal environment and thermal comfort in urban outdoor spaces. *Science of The Total Environment*, *661*, 337–353. Retrieved from `https://doi.org/10.1016/j.scitotenv.2019.01.062https://linkinghub.elsevier.com/retrieve/pii/S0048969719300683` doi: 10.1016/j.scitotenv.2019.01.062

Li, D., & Bou-Zeid, E. (2013). Synergistic interactions between urban heat islands and heat waves: The impact in cities is larger than the sum of its parts. *Journal of Applied Meteorology and Climatology*, *52*(9), 2051–2064. doi: 10.1175/JAMC-D-13-02.1

Li, D., Bou-Zeid, E., & Oppenheimer, M. (2014, may). The effectiveness of cool and green roofs as urban heat island mitigation strategies. *Environmental Research Letters*, *9*(5), 055002. Retrieved from `https://iopscience.iop.org/article/10.1088/1748-9326/9/5/055002` doi: 10.1088/1748-9326/9/5/055002

Louis, J. F. (1979). A parametric model of vertical eddy fluxes in the atmosphere. *Boundary-Layer Meteorology*, *17*(2), 187–202. doi: 10.1007/BF00117978

Martilli, A. (2014, dec). An idealized study of city structure, urban climate, energy consumption, and air quality. *Urban Climate*, *10*(P2), 430–446. Retrieved from `http://dx.doi.org/10.1016/j.uclim.2014.03.003https://linkinghub.elsevier.com/retrieve/pii/S2212095514000200` doi: 10.1016/j.uclim.2014.03.003

Martilli, A., Clappier, A., & Rotach, M. W. (2002). An Urban Surface Exchange Parametrization for Mesoscale Models. *Boundary-Layer Meteorology*, *104*(2), 261–304.

Masson, V. (2000, mar). A Physically-Based Scheme For The Urban Energy Budget In Atmospheric Models. *Boundary-Layer Meteorology*, *94*(3), 357–397. Retrieved from `http://link.springer.com/10.1023/A:1002463829265` doi: 10.1023/A:1002463829265

Masson, V., Bonhomme, M., Salagnac, J.-L., Briottet, X., & Lemonsu, A. (2014, jun). Solar panels reduce both global warming and urban heat island. *Frontiers in Environmental Science*, *2*(June), 1–10. Retrieved from `http://journal.frontiersin.org/Journal/10.3389/fenvs.2014.00014/full{\%}5Cnhttp://journal.frontiersin.org/article/10.3389/fenvs.2014.00014/abstracthttp://journal.frontiersin.org/article/10.3389/fenvs.2014.00014/abstract` doi: 10.3389/fenvs.2014.00014

Mlawer, E. J., Taubman, S. J., Brown, P. D., Iacono, M. J., & Clough, S. A. (1997, jul). Radiative transfer for inhomogeneous atmospheres: RRTM, a validated correlated-k model for the longwave. *Journal of Geophysical Research: Atmospheres*, *102*(D14), 16663–16682. Retrieved from `http://doi.wiley.com/10.1029/97JD00237` doi: 10.1029/97JD00237

Niu, G. Y., Yang, Z. L., Mitchell, K. E., Chen, F., Ek, M. B., Barlage, M., ... Xia, Y. (2011). The community Noah land surface model with multiparameterization options (Noah-MP): 1. Model description and evaluation with local-scale measurements. *Journal of Geophysical Research Atmospheres*, *116*(12), 1–19. doi: 10.1029/2010JD015139

NREL. (2020). *Best Research-Cell Efficiencies Chart.* Retrieved 2020-02-12, from `https://www.nrel.gov/pv/cell-efficiency.html`

Oke, T. R., Mills, G., Christen, A., & Voogt, J. A. (2017). *Urban Climates.* Cambridge: Cambridge University Press. Retrieved from `http://ebooks.cambridge.org/ref/id/CBO9781139016476` doi: 10.1017/9781139016476

Pappaccogli, G., Giovannini, L., Cappelletti, F., & Zardi, D. (2018). Challenges in the application of a WRF/Urban-TRNSYS model chain for estimating the cooling demand of buildings: A case study in Bolzano (Italy). *Science and Technology for the Built Environment*, *24*(5), 529–544. doi: 10.1080/23744731.2018.1447214

Pappaccogli, G., Giovannini, L., Zardi, D., & Martilli, A. (2020, dec). Sensitivity analysis of urban microclimatic conditions and building energy consumption on urban parameters by means of idealized numerical simulations. *Urban Climate*, *34* (April), 100677. Retrieved from https://doi.org/10.1016/j.uclim.2020.100677https://linkinghub.elsevier.com/retrieve/pii/S2212095519304213 doi: 10.1016/j.uclim.2020.100677

Salamanca, F., Georgescu, M., Mahalov, A., Moustaoui, M., & Martilli, A. (2016). Citywide Impacts of Cool Roof and Rooftop Solar Photovoltaic Deployment on Near-Surface Air Temperature and Cooling Energy Demand. *Boundary-Layer Meteorology*. Retrieved from http://link.springer.com/10.1007/s10546-016-0160-y doi: 10.1007/s10546-016-0160-y

Salamanca, F., Krpo, A., Martilli, A., & Clappier, A. (2010). A new building energy model coupled with an urban canopy parameterization for urban climate simulations-part I. formulation, verification, and sensitivity analysis of the model. *Theoretical and Applied Climatology*, *99* (3-4), 331–344. doi: 10.1007/s00704-009-0142-9

Salamanca, F., Zhang, Y., Barlage, M., Chen, F., Mahalov, A., & Miao, S. (2018, mar). Evaluation of the WRF-Urban Modeling System Coupled to Noah and Noah-MP Land Surface Models Over a Semiarid Urban Environment. *Journal of Geophysical Research: Atmospheres*, *123* (5), 2387–2408. Retrieved from http://doi.wiley.com/10.1002/2018JD028377 doi: 10.1002/2018JD028377

Santamouris, M. (2014, may). Cooling the cities – A review of reflective and green roof mitigation technologies to fight heat island and improve comfort in urban environments. *Solar Energy*, *103*, 682–703. Retrieved from http://dx.doi.org/10.1016/j.solener.2012.07.003https://linkinghub.elsevier.com/retrieve/pii/S0038092X12002447 doi: 10.1016/j.solener.2012.07.003

Scherba, A., Sailor, D. J., Rosenstiel, T. N., & Wamser, C. C. (2011). Modeling impacts of roof reflectivity, integrated photovoltaic panels and green roof systems on sensible heat flux into the urban environment. *Building and Environment*, *46* (12), 2542–2551. doi: 10.1016/j.buildenv.2011.06.012

Short, D., Dawes, R. W., & White, I. (1995). The practicability of using Richards' equation for general purpose soil-water dynamics models. *Environment International*, *21* (5), 723–730. Retrieved from https://doi.org/10.1016/0160-4120(95)00065-S doi: 10.1016/0160-4120(95)00065-S

Skamarock, W., Klemp, J., Dudhia, J., Gill, D., Zhiquan, L., Berner, J., . . . Huang, X.-Y. (2019). A Description of the Advanced Research WRF Model Version 4. *NCAR Technical Note NCAR/TN-475+STR*, 145. Retrieved from http://library.ucar.edu/research/publish-technote doi: 10.5065/1dfh-6p97

Stamnes, K., Tsay, S. C., Wiscombe, W., & Jayaweera, K. (1988, jun). Numerically stable algorithm for discrete-ordinate-method radiative transfer in multiple scattering and emitting layered media. *Applied optics*, *27* (12), 2502–9. Retrieved from http://journals.ametsoc.org/doi/abs/10.1175/1520-0469{\%}281989{\%}29046{\%}3C3077{\%}3ANSOCOD{\%}3E2.0.CO{\%}3B2http://www.ncbi.nlm.nih.gov/pubmed/20531783 doi: 10.1364/AO.27.002502

UNI/TS 11300–1. (2014). *Energy Performance of Buildings Part 1: Evaluation of Energy Need for Space Heating and Cooling Rome.* (No. 0).

US Department of Energy. (2010). EnergyPlus Engineering Reference: The Reference to EnergyPlus Calculations. *US Department of Energy* (c), 868. Retrieved from http://scholar.google.com/scholar?hl=en{\&}btnG=Search{\&}q=intitle:EnergyPlus+Engineering+Reference,+The+Reference+to+EnergyPlus+Calculations{\#}1 doi: citeulike-article-id:10579266

Yang, L., Yan, H., & Lam, J. C. (2014, feb). Thermal comfort and building energy consumption implications – A review. *Applied Energy*, *115*, 164–173. Retrieved from `http://dx.doi.org/10.1016/j.apenergy.2013.10.062https://linkinghub.elsevier.com/retrieve/pii/S0306261913008921` doi: 10.1016/j.apenergy.2013.10.062

Zonato, A., Martilli, A., Di Sabatino, S., Zardi, D., & Giovannini, L. (2020). Evaluating the performance of a novel WUDAPT averaging technique to define urban morphology with mesoscale models. *Urban Climate*, *31*. doi: 10.1016/j.uclim.2020.100584